FUNCTION™ american physiological society

FUNCTION, 2022, 3(4): zqac027

https://doi.org/10.1093/function/zqac027
Advance Access Publication Date: 23 May 2022
Original Research

RESEARCH ARTICLE

Muscle-Specific Cellular and Molecular Adaptations to Late-Life Voluntary Concurrent Exercise

Cory M. Dungan[1,2,†], Camille R. Brightwell[2,3,†], Yuan Wen[1,2], Christopher J. Zdunek[2], Christine M. Latham[2,3], Nicholas T. Thomas[2,3], Alyaa M. Zagzoog[2,3], Benjamin D. Brightwell[4], Georgia L. VonLehmden[2], Alexander R. Keeble[2,3], Stanley J. Watowich[5], Kevin A. Murach[2,6,7,*], Christopher S. Fry[2,3,*]

[1]Department of Physical Therapy, University of Kentucky, Lexington 40536, KY, USA, [2]Center for Muscle Biology, University of Kentucky, Lexington 40536, KY, USA, [3]Department of Athletic Training and Clinical Nutrition, University of Kentucky, Lexington 40536, KY, USA, [4]Kinesiology and Health Promotion Graduate Program, University of Kentucky, Lexington 40536, KY, USA, [5]Department of Biochemistry and Molecular Biology, University of Texas Medical Branch, Galveston 77555, TX, USA, [6]Department of Health, Human Performance, and Recreation, University of Arkansas, Fayetteville 72701, AR, USA and [7]Cell and Molecular Biology Program, University of Arkansas, Fayetteville 72701, AR, USA

*Address correspondence to K.A.M. (e-mail: kmurach@uark.edu), C.S.F. (cfr223@uky.edu)
†indicates co-first author

Abstract

Murine exercise models can provide information on factors that influence muscle adaptability with aging, but few translatable solutions exist. Progressive weighted wheel running (PoWeR) is a simple, voluntary, low-cost, high-volume endurance/resistance exercise approach for training young mice. In the current investigation, aged mice (22-mo-old) underwent a modified version of PoWeR for 8 wk. Muscle functional, cellular, biochemical, transcriptional, and myonuclear DNA methylation analyses provide an encompassing picture of how muscle from aged mice responds to high-volume combined training. Mice run 6–8 km/d, and relative to sedentary mice, PoWeR increases plantarflexor muscle strength. The oxidative soleus of aged mice responds to PoWeR similarly to young mice in every parameter measured in previous work; this includes muscle mass, glycolytic-to-oxidative fiber type transitioning, fiber size, satellite cell frequency, and myonuclear number. The oxidative/glycolytic plantaris adapts according to fiber type, but with modest overall changes in muscle mass. Capillarity increases markedly with PoWeR in both muscles, which may be permissive for adaptability in advanced age. Comparison to published PoWeR RNA-sequencing data in young mice identified conserved regulators of adaptability across age and muscles; this includes *Aldh1l1* which associates with muscle vasculature. *Agrn* and *Samd1* gene expression is upregulated after PoWeR simultaneous with a hypomethylated promoter CpG in myonuclear DNA, which could have implications for innervation and capillarization. A promoter CpG in *Rbm10* is hypomethylated by late-life

Submitted: 30 April 2022; **Revised:** 6 May 2022; **Accepted:** 8 May 2022

© The Author(s) 2022. Published by Oxford University Press on behalf of American Physiological Society. This is an Open Access article distributed under the terms of the Creative Commons Attribution-NonCommercial License (https://creativecommons.org/licenses/by-nc/4.0/), which permits non-commercial re-use, distribution, and reproduction in any medium, provided the original work is properly cited. For commercial re-use, please contact journals.permissions@oup.com

exercise in myonuclei, consistent with findings in muscle tissue. PoWeR and the data herein are a resource for uncovering cellular and molecular regulators of muscle adaptation with aging.

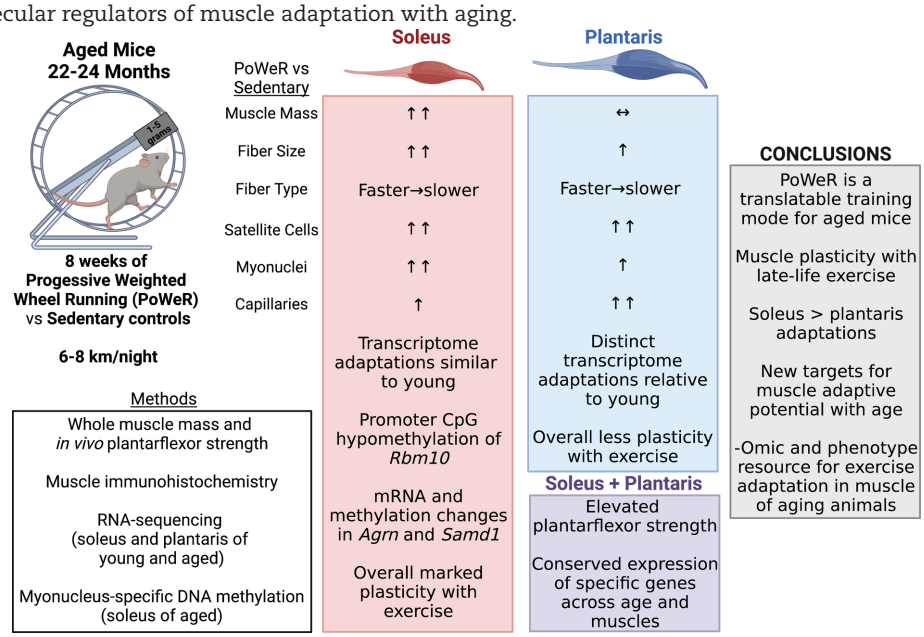

Key words: hypertrophy; capillarization; sarcopenia; concurrent training; skeletal muscle; DNA methylation

Introduction

Age-related atrophy of skeletal muscle and the concomitant decline in muscle strength and physical function, termed sarcopenia, directly contributes to the development of progressive disability.[1,2] To combat the sarcopenic decline into disability, clinical exercise studies have sought to optimize loading-induced skeletal muscle hypertrophy in older adults. Resistance or endurance exercise can be an effective countermeasure to combat sarcopenia,[3–8] but regardless of the intervention, skeletal muscle adaptive potential is almost always blunted in older populations.[9] Solving the problem of "anabolic resistance" with aging has proven challenging. Human exercise studies are limited by muscle tissue availability when aiming to comprehensively evaluate mechanisms mediating or limiting loading-induced hypertrophy, strength gain, and cellular adaptations. Furthermore, carrying out late-life exercise trials in humans presents various challenges, not limited to locating the appropriate participant population and issues of adherence.[10,11]

Translatable pre-clinical murine models of *bona fide* growth-inducing exercise have historically been lacking. This barrier hampers our ability to uncover targetable molecular transducers of exercise adaptation with aging; we summarize the recent available approaches in young and aged mice here.[12] To date, most murine investigations studying muscle hypertrophy with aging employed the synergist ablation surgical approach. Synergist ablation is invasive, non-translatable to humans, and only allows for the study of one fast-twitch muscle (plantaris or extensor digitorum longus) that primarily contains myosin heavy chain Type 2b fibers not present in human skeletal muscle.[12,13] Since loading is constant and strenuous in this model, muscle hypertrophy can be extremely rapid and pronounced in young mice,[14,15] yet almost completely absent in aged mice (24 mo old);[16] resistance exercise training without adequate rest and recovery is deleterious to maximizing muscle adaptation in aged muscle.[17] Recent attempts at combining a synergist denervation model with forced treadmill running[18,19] yielded some positive results in aged mouse muscle.[19] This surgical/running approach is still restricted to one muscle type, is strenuous, and minimally translatable to humans. The development of a resistive self-paced murine exercise model that targets diverse muscles and allows for voluntary rest could circumvent issues associated with prior approaches.

The current recommendation from the American College of Sports Medicine is combined endurance and resistance exercise to improve overall health and wellbeing.[20] In untrained humans, combined (or concurrent) exercise training where endurance and resistance adaptations occur in the same training program can be advantageous for aspects of muscle adaptation, including mass accrual.[21,22] As such, a combined modality voluntary murine exercise model for young mice called progressive weighted wheel running (PoWeR) was recently developed by Dungan and Murach et al.[23,24] PoWeR involves modifying standard metal running wheels in an unbalanced fashion with 1-gram magnetic weights. This approach improves on prior wheel-running protocols that utilized a friction-based loading strategy,[12,25,26] does not require significant human oversight or intervention,[27–29] does not use feeding as a reward for performing the activity[30], allows for simultaneous combined endurance/resistance exercise training, and produces marked muscle cellular-level hypertrophy and fiber-type adaptations across muscle groups of young mice. Importantly, PoWeR adaptations extend to the soleus, which contains the myosin fiber types predominantly found in humans.[23,24,31–35] We summarize whole muscle and cellular adaptations (fiber size, myosin type distribution, satellite cell and myonuclear number) to PoWeR in young adult C57BL/6 mice (4–6 mo old) in Supplemental Table 1. The purpose of the current investigation was to leverage a

modified version of PoWeR in aged mice to study the whole muscle, cellular, and molecular underpinnings of exercise adaptation late in life. We also provide muscle- and nucleus-specific -omics data as a resource for the field. We hypothesized that PoWeR in old mice, characterized by gradual loading, voluntary rest periods, and a simultaneous concurrent training-like stimulus in several muscles would promote skeletal muscle plasticity in aged muscle. Muscle capillarity is related to muscle fiber size.[36,37] Capillary adaptations are mechanistically necessary for loading-induced muscle fiber hypertrophy in young mice,[38] and are emerging as a key factor associated with muscle growth during aging.[39–43] Therefore, we also tested whether a conserved adaptive response to PoWeR would correspond with several different measures of capillarization.

Materials and methods

Ethical approval

Animal procedures were approved by the Institutional Animal Care and Use Committee at the University of Kentucky. All mice were singly housed in the same temperature and humidity-controlled room on a 12h:12h light–dark cycle. Mice were given *ad libitum* access to food and water and were euthanized by cervical dislocation under deep anesthesia.

Experimental design

Twenty-two-month-old female C57BL/6N mice were obtained from the Charles River Laboratories National Institute of Aging research colony. Mice were randomly assigned to the PoWeR or sedentary control group. Mice in the PoWeR group were singly housed in cages with running wheels to monitor individual running volume using ClockLab software. Mice in the sedentary group were singly housed in cages without running wheels. Following an introductory week with an unweighted wheel, 8 wk of PoWeR training commenced with the following weight progression: 2 g in week 1, 3 g in week 2, 4 g in week 3, and 5 g in weeks 4–8. One-gram magnets (product no. B661, K&J Magnetics, Pipersville, PA) were affixed to one side of the wheel to allow for the progressive increase in weight. As previously described,[23] the asymmetrical loading pattern of the weight produced an unbalanced wheel, resulting in frequent stopping and restarting of running, which forced the mice to overcome the wheel's weight repeatedly instead of relying on momentum after the initial starting effort. Mice were 24 mo old upon completion of the experiment. The PoWeR protocol was modified based upon the PoWeR protocol previously reported to be effective in eliciting hypertrophy in young mice.[23,24] Prior to functional assessment and tissue harvest, wheels were locked for 24 h for mice in the PoWeR group, along with an overnight fast for all mice. Following 8 wk of PoWeR or in sedentary controls, the contractile function of plantar flexors was assessed on the right hind limb, and mice were humanely euthanized by cervical dislocation under deep anesthesia. Plantar flexor muscles (soleus, plantaris, and gastrocnemius) were rapidly dissected. Muscle from the right hind limb was processed for immunohistochemical analyses, and muscle from the left leg was processed for RNA isolation or enzymatic assays.

Immunohistochemistry (IHC)

IHC analyses were performed on soleus, plantaris, and gastrocnemius muscles—comprising the entire plantar flexor complex. Each muscle from the right hind limb was covered in Tissue Tek (O.C.T. Compound, Sakura Finetek, Torrance, CA, USA) at resting length and frozen in liquid nitrogen-cooled 2-methylbutane on a foil-covered cork. Samples were stored at −80°C until analysis. Using a cryostat (HM525-NX, Thermo Fisher Scientific, Waltham, MA, USA), 7 μm-thick sections were cut from each muscle and air dried for 1 h on slides. Slides were stored at −20°C before IHC staining.

For immunofluorescent detection of satellite cells, sections were fixed in 4% paraformaldehyde (PFA) for 10 min at room temperature, followed by washes with phosphate-buffered saline (PBS, pH 7.4). Antigen retrieval was performed with sodium citrate (10mM, pH 6.5) in a 92°C water bath for 20 min. Slides were allowed to cool to room temperature and washed in PBS, followed by blocking of endogenous peroxidases with 3% hydrogen peroxide for 10 min. Slides were then washed in PBS and blocked for 1 h in a mouse-on-mouse Ms IgG blocking solution (cat#MKB-2213, Vector Laboratories) diluted in 2% bovine serum albumin (BSA). Slides were rewashed in PBS and incubated overnight in primary antibodies against Pax7 (mouse IgG1, 1:100; Developmental Studies Hybridoma Bank (DSHB)) and laminin (rabbit IgG, 1:200; L9393, Millipore Sigma) in the 2% BSA at 4°C. The following day, slides were washed in PBS and incubated for 90 min at room temperature in goat anti-mouse biotinylated secondary antibody (1:1000; #115–065–205, Jackson Immuno Research) and goat anti-rabbit secondary antibody directly conjugated to Alexa Fluor 488 (1:250; #A11034, Invitrogen). Slides were washed in PBS and incubated for 1 h at room temperature in streptavidin conjugated to horse radish peroxidase (SA-HRP, Life Technologies/Thermo Fisher Scientific). Following another wash in PBS, Pax7 was amplified by incubation for 15 min at room temperature in TSA-Alexa Fluor 594 (1:500 in PBS; B40957, Invitrogen). Slides were washed in PBS, incubated for 10 min in 4′,6-diamidino-2-phenylindole (DAPI; 10 nM, Life Technologies/Thermo Fisher Scientific), washed again in PBS, and mounted using PBS and glycerol (1:1).

For immunofluorescent assessment of muscle fiber type distribution and fiber type-specific cross-sectional area (CSA) and myonuclei, slides were incubated overnight at 4°C in primary antibodies against dystrophin (rabbit IgG, 1:200; ab15277, Abcam) and myosin heavy chain (MHC) Type 1 (mouse IgG2b, 1:100; BA.D5 concentrate, DSHB) in myosin heavy chain Type 2a supernatant (mouse IgG1; SC.71, DSHB). On the following day, slides were washed in PBS and incubated for 90 min at room temperature in goat anti-mouse IgG1 AF488 secondary antibody (1:250; #A21121, Invitrogen), goat anti-mouse IgG2b AF647 secondary antibody (1:250; #A21242, Invitrogen), and goat anti-rabbit IgG AF568 secondary antibody (1:250; #A11011, Invitrogen) in PBS. Slides were then incubated in DAPI (10nM, Life Technologies/Thermo Fisher Scientific) for 10 min followed by another wash in PBS. Slides were mounted using PBS and glycerol (1:1). The sections for fiber typing were also used for myonuclear analysis.

For immunofluorescent detection of muscle capillaries, sections were fixed in acetone for 10 min at −20°C and washed in PBS. Slides were blocked for 1 h in 2.5% normal horse blocking solution (#S-2012, Vector Laboratories) at room temperature and incubated overnight in primary antibodies against CD31 (rat IgG, 1:100; #550 274, BD Biosciences) and laminin (rabbit IgG, 1:200;

L9393, Millipore Sigma) in 2.5% normal horse serum at 4°C. The following day, slides were washed in PBS and incubated for 1 h in goat anti-rabbit secondary directly conjugated to Alexa Fluor 488 (1:500; #A11034, Invitrogen) and goat anti-rat Cy3 secondary (1:250; #550 274, BD Biosciences) in PBS. Slides were rewashed in PBS followed by incubation in DAPI for 10 min (10nM, Life Technologies/Thermo Fisher Scientific), additional washing in PBS, and mounting with Vectashield fluorescence mounting media (Vector Laboratories, Burlingame, CA, USA).

Fiber-type specific succinate dehydrogenase

About 7 μm-thick sections were cut from samples previously frozen for IHC analyses and placed on slides, as described above. Sections were air dried for 1 h followed immediately by tissue staining. Slides were incubated in a solution of nitrotetrazolium blue (NBT, N6876, Millipore Sigma) and succinate acid disodium (224731, Millipore Sigma) in 0.2 M PBS (pH 7.4) at 37°C for 15 min, followed by rinses in an acetone gradient and distilled water. Slides were mounted with Vectashield fluorescence mounting media (H-1000, Vector Laboratories) and imaged with brightfield. To assess fiber type on the same sections, slides were incubated in PBS to carefully remove the coverslip. Sections were then incubated overnight at room temperature in primary antibodies against dystrophin (rabbit IgG, 1:200; ab15277, Abcam) and myosin heavy chain (MHC) Type 1 (mouse IgG2b, 1:100; BA.D5 concentrate, DSHB) and Type 2a (mouse IgG1, undiluted supernatant, SC.71, DSHB) in PBS. Slides were washed in PBS and incubated for 1 h at room temperature in goat anti-mouse IgG2b AF647 secondary antibody (1:250; #A21242, Invitrogen), goat anti-mouse IgG1 AF488 secondary antibody (1:250; #A21121, Invitrogen) and goat anti-rabbit IgG AF568 secondary antibody (1:250; #A11011, Invitrogen) in PBS. Slides were washed in PBS and post-fixed in methanol at room temperature for 5 min, followed by a final wash in PBS before mounting with Vectashield fluorescence mounting media (H-1000, Vector Laboratories).

Image acquisition and analysis

Images were captured at 100–200x magnification with a Zeiss upright microscope (AxioImager M1; Zeiss, Oberkochen, Germany). Image analysis was performed in a blinded manner by the same assessor using Zen Blue software for manual counting of satellite cells. Satellite cells were identified as Pax7+/DAPI + within the laminin border. Myofibers were manually counted, and satellite cell number was normalized per 100 myofibers. MyoVision software was used for automated analysis of myonuclear density normalized to myofiber number, fiber type distribution, and fiber type-specific CSA.[23] Unstained myofibers were counted as MHC IIx + IIb fibers. Zen Blue was used for manual analysis of all capillary indices, which were calculated as previously reported.[5] Briefly, capillary contacts were counted as the total number of capillaries in contact with the myofiber. The capillary-to-fiber ratio was calculated as the number of capillaries divided by a sharing factor (the number of myofibers sharing the same capillary). The capillary-to-fiber-perimeter-exchange index was measured as the supply of capillaries relative to the myofiber perimeter (capillary-to-fiber ratio/perimeter of the myofiber). The index of the capillary to fiber interface was calculated as the percentage of the capillary in contact with the myofiber.

In Vivo plantar flexor peak torque

Upon completion of 8 wk of PoWeR training or the sedentary control period, the strength of the plantar flexor muscle complex was assessed in the 24-mo-old mice by in vivo isometric peak tetanic torque, similar to our prior published methods.[31] In an induction chamber, mice were anesthetized with 2.5% isoflurane vaporized in 1.5 L/min oxygen (VetEquip vaporizer). Mice were then transferred to a secure nose cone with a continuous flow of isoflurane in oxygen. The right hind limb was analyzed for all mice, and fur was trimmed (Wahl Bravmini, Wahl Corporation) to ensure unobstructed electrode placement. Mice were placed in the supine position on a 37°C temperature regulated platform (809c in-situ mouse apparatus, Aurora Scientific, Aurora, ON, Canada), and the hind limb was secured using a clamp at the knee with the foot placed in a footplate on a dual-mode lever and motor (300D-300C-LRFP, Aurora Scientific). Surgical tape was wrapped around the foot secured to the footplate to prevent movement of the heel of placement shifting, and the footplate and motor arm was adjusted to place the tibia parallel with the platform with a 90-degree angle at the ankle. Needle electrodes were positioned percutaneously slightly lateral to the knee to maximally stimulate the tibial nerve using an electrical stimulator (High Power Bi-Phase Stimulator, Aurora Scientific). Using repeated twitches with the Instant Stimulation function with Live View in Dynamic Muscle Control LabBook (DMC v6.000), placement of needle electrodes was adjusted to optimize location to generate maximum isometric torque and eliminate antagonistic dorsiflexion. Optimal amperage to produce maximal torque was determined by a progressive series of twitch experiments (0.05 s stimulus duration) beginning with 10 mA and increasing in small increments until the maxim torque stimulated by the minimum amperage was recorded. The amperage then remained constant throughout the force-frequency experiment (10, 40, 80, 120, 150, 180, and 200 Hz, 0.25s stimulus duration with a 2 min rest period between each stimulus) from which isometric peak tetanic torque was recorded. Peak torque data were collected using DMC v6.000 and analyzed with Dynamic Muscle Analysis software (DMA v5.501). The rate of torque development was calculated using custom Matlab code (MATLAB R2019a) with raw data files generated from the contraction in the force-frequency curve at which peak torque occurred. The rate of torque development was calculated from the starting threshold to 10, 20, 50, and 75 ms. Plantar flexor isometric peak tetanic torque is reported as peak torque normalized to body mass (mN∗m/g).

Citrate synthase (CS) and cytochrome C oxidase (CCO) activity assays

Flash frozen soleus muscle was cryopulverized into a fine powder (BioPulverizer; Biospec Products Inc., Bartlesville, OK) for evaluation for CS and CCO activities as markers of mitochondrial volume density and function, respectively.[44,45] Samples were prepared and activities were measured as previously described.[46,47] Briefly, CS activity was assessed at 412 nm by measuring the initial reaction rate of free CoA-SH with DTNB; CCO activity was determined by measuring the maximal, linear rate of oxidation of fully reduced cytochrome c at 550 nm. Enzymatic activities were normalized to homogenate supernatant protein content, determined using the Bio-Rad Protein Assay Dye Reagent (Bio-Rad Laboratories, Herculese, CA) and albumin

standard (Thermo Scientific, Waltham, MA). Cytochrome c oxidase activity is presented on an integrative (per mg protein) and intrinsic (per unit CS) basis.

RNA isolation and RNA-sequencing (RNA-seq)

Muscle from the left hind limb was flash frozen in liquid nitrogen and stored at −80°C. Soleus and plantaris muscles were homogenized (n: Control = 5, PoWeR = 4 for both plantaris and soleus; samples were not pooled) in TRI Reagent (R2050-1-200, Zymo Research). RNA was isolated using the Direct-zol RNA Miniprep kit (R2051, Zymo Research) per manufacturer's instructions. RNA concentration and quality (RIN > 8.1) was assessed with an RNA Nano chip kit on a bioanalyzer by the University of Kentucky Genomics Core Laboratory. Isolated RNA was sent to Novogene for library construction, sequencing, and preliminary bioinformatic analyses. FASTQ files were aligned using STAR aligner in Partek and analyzed and normalized using DESeq2 (minimum read cutoff of 50 across all samples). RNA-sequencing previously published by Englund et al.,[31] also performed by Novogene, was analyzed separately using the same pipeline for comparison to our aging PoWeR data. These mice (n = 4/group) were 4-mo-old vehicle-treated Pax7-DTA mice (C57BL/6 background) that were PoWeR trained for 8 weeks with up to 6 grams of resistance, and soleus and plantaris tissue was harvested after an overnight fast (control and PoWeR) and 24-h wheel-lock (PoWeR mice). *P* values were adjusted using the Benjamini–Hochberg FDR step-up method. Pathway over-representation analysis was performed using gProfiler [48,49] with non-ordered query and up-or-downregulated genes with FDR < 0.10; all KEGG, Reactome, and WikiPathway pathways reported had Benjamini–Hochberg adjusted *P* values < 0.05.

Myonuclear-specific low-input reduced representation bisulfite sequencing (RRBS)

Male HSA-rtTA$^{+/-}$; H2B-GFP$^{+/-}$ (HSA-GFP) mice were generated as previously described by us[33–35,50,51] and aged until 22 mo. One cohort of adult mice was treated with low-dose doxycycline (0.5 mg/mL doxycycline in drinking water with 2% sucrose) during the last week of eight weeks of voluntary PoWeR exercise (biological triplicate) as described previously;[33,34] myonuclear labeling late in training results in the capture of resident as well as satellite cell-derived myonuclei.[33] A second cohort remained sedentary in their cages without a wheel (biological triplicate) and were treated with doxycycline at the same time as PoWeR mice. After eight weeks, myonuclei from soleus muscles were processed via Dounce homogenization in a physiological buffer following a 24-h wheel lock and overnight fast, purified via fluorescent activated myonuclear sorting (GFP + and had incorporated propidium iodide), then analyzed using myonucleus-specific low-input RRBS, as described by us.[34,50,52] We modified our prior protocol slightly by filtering samples then sorting directly into buffer ATL with proteinase K, omitting any centrifugation steps, which maximized yield. Myonuclear DNA was extracted using the Qiagen DNA MicroKit (Hilden, Germany) with carrier RNA, and low-input Msp1 RRBS was performed by Zymo Research using 10 ng of genomic DNA (Irvine, California, USA).[34,50] RRBS data were processed using MethylSig,[53] with a minimum cutoff of 10x coverage per CpG site in each sample.[34] Promoters were defined as within 1 kb upstream of the transcription start site.[34] Differentially methylated sites were determined using a beta binomial distribution and a false discovery rate (FDR) <0.10, as determined by the Benjamini–Hochberg method.

Statistical analysis

All statistical analyses were performed using GraphPad Prism version 7.00 for Mac OS X (GraphPad Software, La Jolla, CA). Data were checked for normality and original or log transformed data were used. For each outcome, unpaired t-tests were utilized to detect statistically significant differences between PoWeR and control groups. FDR for sequencing experiments was set at < 0.10. All data are reported as mean ± standard error of the mean (SEM). Effect sizes were calculated using Cohen's D.

Results

Over the 8-wk period, the wheel was gradually loaded up to 5 g; a maximum of 6 g was used previously in young mice.[23,24] Mice (n = 10) ran an average of 6.35 ± 0.72 km/d, with a peak average of 8.20 ± 1.04 km/d at Week 2 (Figure 1A). Body weight was lower in PoWeR mice relative to age-matched sedentary (n = 14) (Figure 1B), and heart weight normalized to body weight was heavier after PoWeR (+11%, *P* = 0.01, effect size [ES] = 1.52, data not shown).

8-wk of PoWeR in aged mice resulted in greater muscle mass in the soleus and fiber CSA in several muscles

Body weight normalized soleus wet weight was elevated in old mice subjected to PoWeR (+13%, *P* = 0.01, ES = 1.00, Figure 1C), whereas plantaris (Figure 1D) and gastrocnemius (data not shown) weights were not altered.

For all immunohistochemistry (IHC) analyses, entire muscle cross-sections were used (622 ± 35 fibers for soleus, 607 ± 27 fibers for plantaris, and 4616 ± 202 fibers for gastrocnemius), and most parameters were measured using semi-automated analysis software.[54,55] In soleus muscles of PoWeR mice, there were significantly more Type 1 (oxidative slow-twitch) fibers (+17%, *P* = 0.001, ES = 1.29) with a concomitant decrease in Type 2a (oxidative fast-twitch) fibers (−31%, *P* = 0.01, ES = −1.25) and no change in the relative frequency of 2x + 2b (glycolytic fast-twitch) fibers (Figure 2A-100) relative to sedentary controls. PoWeR resulted in elevated mean fiber CSA in the soleus (+12%, *P* = 0.01, ES = 1.04, Figure 2D), corresponding with larger CSA in Type 1 (+9%, *P* = 0.04, ES = 0.85) and 2a (+16%, *P* = 0.01, ES = 1.07), but not relatively scarce 2x + 2b fibers (Figure 2E). In the plantaris, PoWeR mice had significantly more Type 2a fibers (+39%, *P* < 0.001, ES = 1.50) and fewer Type 2x + 2b fibers (−39%, *P* < 0.001, ES = −1.52, Figure 2F-H). There was no difference in the relative frequency of Type 1 fibers (Figure 2H). Mean muscle fiber CSA in the plantaris was + 10% higher (Figure 2I, *P* = 0.08, ES = 0.73), with larger 2a (+33%, *P* < 0.001, ES = 1.45) and 2x + 2b fibers (+12%, *P* = 0.04, ES = 0.83, Figure 2J). CSA was not altered with PoWeR in the low abundance Type 1 fibers of the plantaris (Figure 2J). Similar to the plantaris, the gastrocnemius exhibited decreased frequency of Type 2x + 2b fibers (-10%, *p* = 0.001, ES = -1.28), an elevated frequency of Type 2a fibers (+50%, *p*<0.001, ES = 1.36), and a non-significant near-doubling of Type 1 fibers (Supplemental Figure 1A-C). The overall mean CSA of the gastrocnemius was not altered by PoWeR (Supplemental Figure 1D), and only Type 2a fibers were significantly larger in response to PoWeR (+19%, *P* = 0.03, ES = 0.91, Supplemental Figure 1E). Collectively, old PoWeR mice display hypertrophic and fiber type distribution adaptations that are in line with those observed in young mice (see Supplemental Table 1), albeit smaller in magnitude in the plantaris muscle specifically.[23,24]

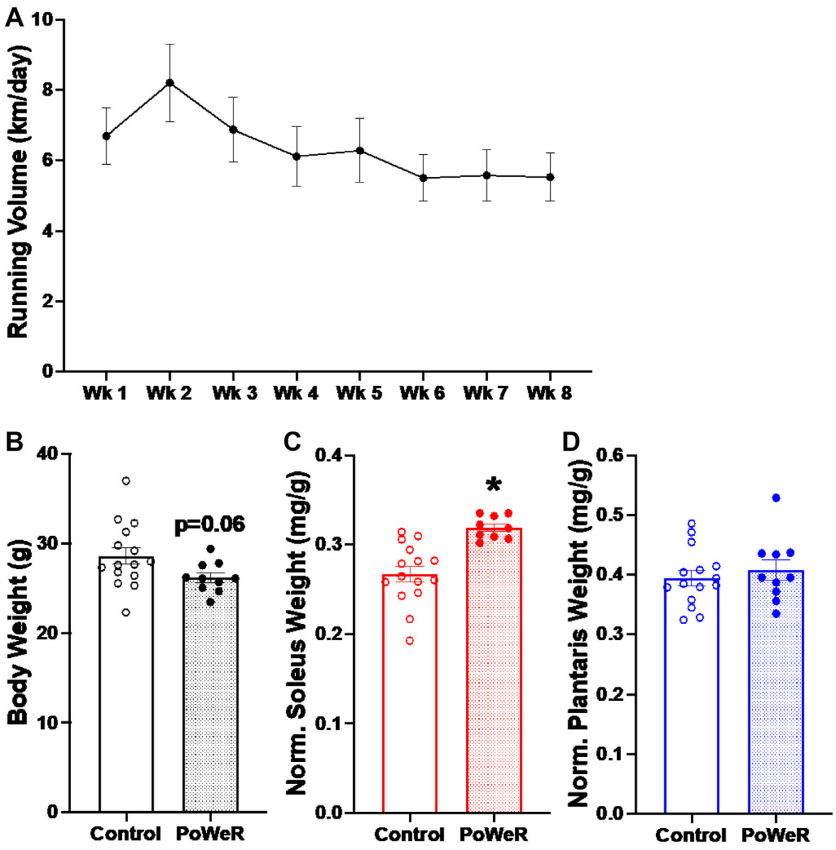

Figure 1. *Voluntary running volume, body weight, and plantar flexor wet weight adaptations to PoWeR.* **(A)** Voluntary running volume of old mice throughout 8 wk of PoWeR. **(B)** Body weight in grams. **(C)** Soleus wet weight normalized to body weight. **(D)** Plantaris wet weight normalized to body. Open bars = control mice, dotted bars = PoWeR mice. $*$ indicates $P < 0.05$. Error bars represent standard error of the mean (SEM). N = 10–15 per group.

Citrate synthase and cytochrome C oxidase activity tracked with fiber type transitions

Due to the robust faster-to-slower fiber-type shift in all muscles in response to PoWeR, we examined indices of mitochondrial content and function in the soleus muscle. Citrate synthase activity, a measure of oxidative adaptation, was reduced in PoWeR mice compared to control mice (−40%, $P < 0.001$, ES = −1.53, Supplemental Figure 2A), while integrative and intrinsic cytochrome C oxidase activities were not different between PoWeR and control mice (Supplemental Figure 2B and C). Type 2a fibers are reported to be more oxidative than Type 1 fibers in mice,[56] which we confirmed by co-staining fiber type with succinate dehydrogenase (SDH) (Supplemental Figure 3). A reduction in mitochondrial volume density with PoWeR could be due to an increase in the less oxidative Type 1 fibers in the soleus.

Satellite cell abundance and myonuclear number was greater across muscles in response to PoWeR

Following PoWeR, both the soleus (Figure 3A-B) and plantaris (Figure 3C-D) had more satellite cells (+37%, $P < 0.001$, ES = 1.58, and 47%, $P = 0.001$, ES = 1.31, respectively), with a 21% difference in the gastrocnemius ($P = 0.14$, effect size = 0.69, Supplemental Figure 4A and B). There was a corresponding elevation in myonuclei in the soleus (+24%, $P = 0.004$, ES = 1.16, Figure 4A–C), specifically in Type 1 and 2a fibers (+20%, $P = 0.02$, ES = 0.97, and + 29%, $P = 0.002$, ES = 1.22, respectively, Figure 4D). In contrast, myonuclear number was not significantly higher in the plantaris following PoWeR (+14%, $P = 0.14$, ES = 0.62, Figure 4E and F). Type 2a fibers had significantly more myonuclei in response to PoWeR (+25%, $P = 0.02$, ES = 0.91, Figure 4H), while the difference in Type 2x + 2b fibers was not significant (Figure 4H, $P = 0.12$, ES = 0.64). The gastrocnemius had 21% more myonuclei following training ($P = 0.07$, ES = 0.77, Supplemental Figure 4C–E), which was primarily driven by the increase in Type 2a (+31%, $P = 0.008$, ES = 1.064, Supplemental Figure 4F) and 2x + 2b fibers (+21%, $P = 0.04$, ES = 0.84, Supplemental Figure 4F), and less contribution from Type 1 fibers ($P = 0.063$, ES = 0.80, Supplemental Figure 4F). There was no difference in the relative number of fibers with centrally located myonuclei in soleus (Control: 1.4 ± 0.6%, PoWeR: 1.7 ± 0.8%), plantaris (Control: 2.2 ± 0.7%, PoWeR: 3.0 ± 1.1%), or gastrocnemius (Control: 1.9 ± 0.4%, PoWeR: 1.7 ± 0.7%) (data not shown); however, since this analysis was a snapshot in time, we cannot exclude the possibility that central myonuclei had moved to the periphery by the time the mice were euthanized. Together, these data demonstrate that PoWeR training in old mice causes similar adaptations to satellite cell abundance and myonuclear accretion as in young mice (see Supplemental Table 1).

PoWeR mice had higher capillary density

In response to PoWeR, we quantified capillary density in the soleus as capillary contacts per fiber (contacts/fiber) (+18%,

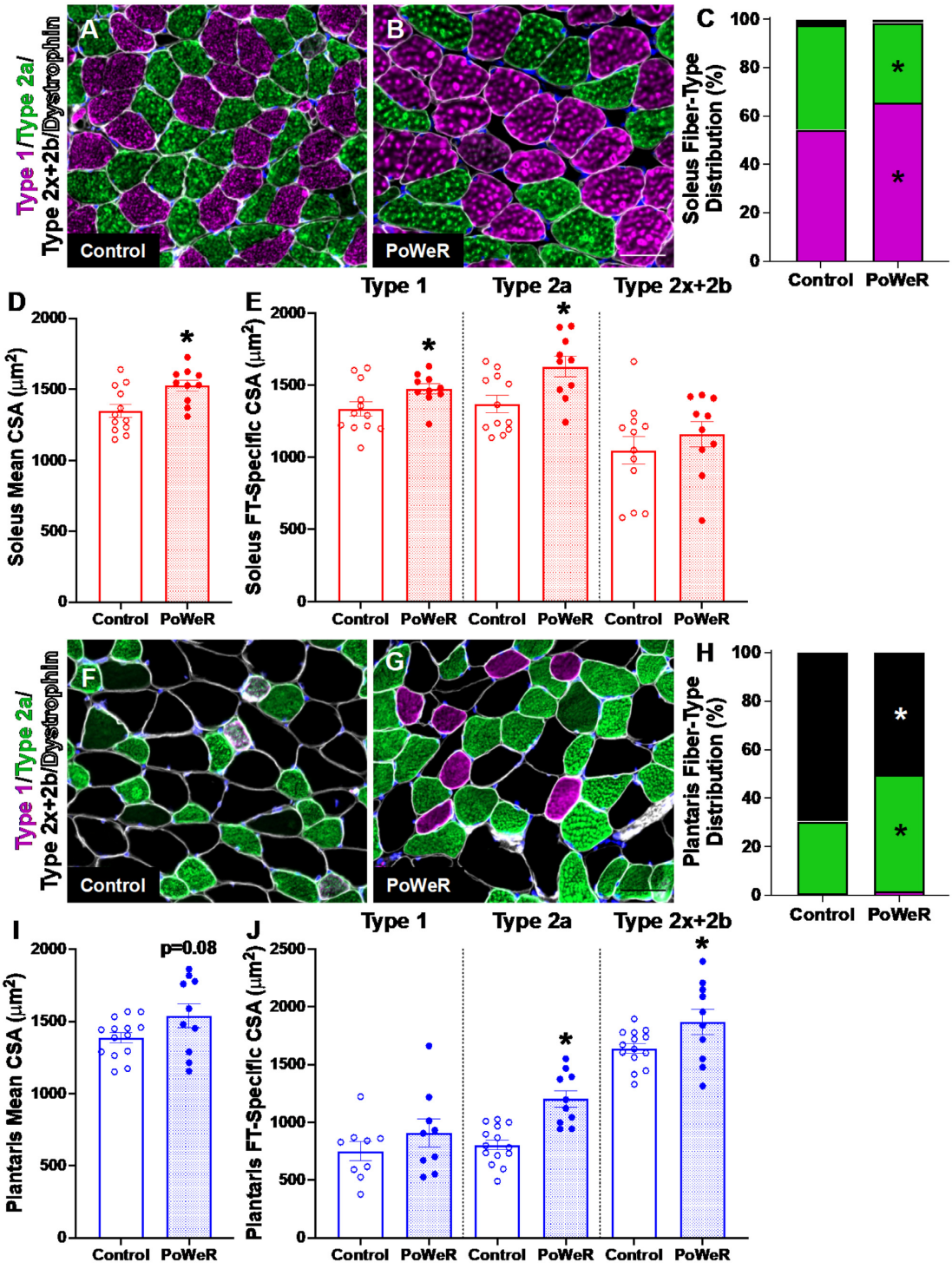

Figure 2. *Changes in muscle fiber type and size following PoWeR.* Representative images of Type 1 (pink), Type 2a (green), Type 2x + 2b (black) and dystrophin (white) immunohistochemistry (IHC) in the soleus from **(A)** control and **(B)** PoWeR trained old mice. **(C)** Soleus fiber-type distribution. **(D)** Soleus mean fiber CSA. **(E)** Soleus fiber-type specific (Type 1, Type 2a, and Type 2x + 2b) CSA. Representative images of Type 1 (pink), Type 2a (green), Type 2x + 2b (black) and dystrophin (white) IHC in the plantaris from **(F)** control and **(G)** PoWeR trained old mice. **(H)** Plantaris fiber-type distribution. **(I)** Plantaris mean fiber CSA. **(J)** Plantaris fiber-type specific (Type 1, Type 2a, and Type 2x + 2b) CSA. CSA = cross-sectional area. Open bars = control mice, dotted bars = PoWeR mice. ∗ indicates $P < 0.05$. Scale bars = 50 μm. Error bars represent SEM. N = 10–14 per group.

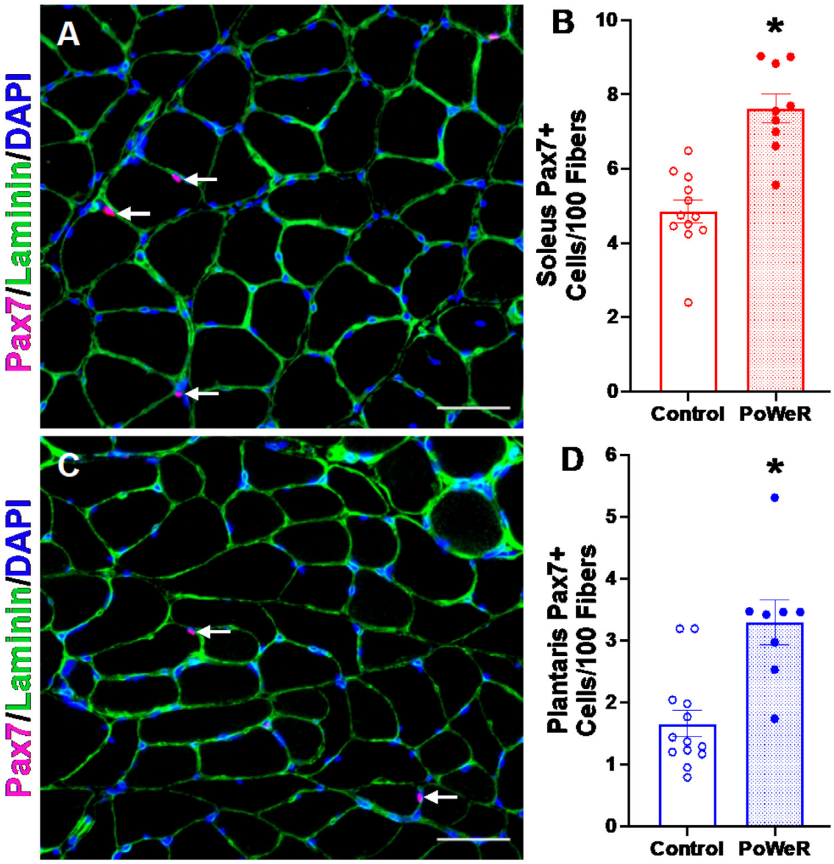

Figure 3. *Satellite cell abundance is elevated in response to PoWeR.* **(A)** Representative images of Pax7 (pink), Laminin (green), and DAPI (blue) IHC in the soleus from control and PoWeR trained old mice. **(B)** Quantification of Pax7 + cells per 100 fibers in the soleus. **(C)** Representative images of Pax7 (pink), Laminin (green), and DAPI (blue) IHC in the plantaris from control and PoWeR trained old mice. **(D)** Quantification of Pax7 + cells per 100 fibers in the plantaris. Open bars = control mice, dotted bars = PoWeR mice. ∗ indicates $P < 0.05$. Scale bars = 50 μm. Error bars represent SEM. N = 9–13 per group.

$P < 0.001$, ES = 1.40) and capillary to fiber ratio relative to a sharing factor (capillaries/fiber) (+10%, $P = 0.04$, ES = 0.95) and saw an elevation in capillary density in response to PoWeR (Figure 5A-D). Capillary to fiber perimeter exchange (CFPE) (+9%, $P = 0.049$, ES = 0.92, Figure 5E) and capillary to fiber interface (LCPF) (+18%, $P = 0.004$, ES = 1.24, Figure 5E) were also improved following PoWeR. In plantaris muscle of PoWeR mice, capillary contacts (+30%, $P < 0.001$, ES = 1.58, Figure 5G–I) and capillary to fiber ratio (+31%, $P < 0.001$, ES = 1.58, Figure 5J) were higher relative to sedentary controls, as were CFPE (+23%, $P = 0.006$, ES = 1.28, Figure 5K) and LCPF (+26%, $P = 0.02$, ES = 1.14, Figure 5L). The change in capillary contacts in gastrocnemius muscles with PoWeR was not significant (Supplemental Figure 5A–C, $P = 0.09$, ES = 0.84), but there was a significant elevation in the capillary to fiber ratio (+24%, $P = 0.03$, ES = 1.04, Supplemental Figure 5D), CFPE (+25%, $P = 0.01$, ES = 1.16, Supplemental Figure 5E), and LCPF (+29%, $P = 0.04$, ES = 0.99, Supplemental Figure 5F). Collectively, these data demonstrate the efficacy of PoWeR to stimulate robust angiogenic adaptations in skeletal muscle from aged mice.

Contractile function was greater with PoWeR

Isometric peak tetanic torque of the plantar flexors was 12% higher in PoWeR mice versus sedentary control mice when normalized to both body weight ($P = 0.0745$, ES = 0.72; Fig 6A) and 11% higher normalized to wet weight of the plantar flexor complex ($P = 0.0702$, ES = 0.73; Fig 6B). PoWeR may elicit a clinically relevant functional adaptation in old mice. The rate of torque development was not statistically different at each calculated time point from the starting threshold in PoWeR mice compared to control mice (10 ms: PoWeR- 140.5 ± 27.6 mN∗m/s, Control- 131.7 39.8 mN∗m/s, $P = 0.5316$, effect size = 0.25; 20 ms: PoWeR- 148.2 ± 30.8 mN∗m/s, Control- 136.7 ± 38.9 mN∗m/s, $P = 0.4278$, ES = 0.32; 50 ms: PoWeR- 103.8 ± 20.5 mN∗m/s, Control- 98.0 ± 25.9 mN∗m/s, $P = 0.5475$, ES = 0.25; 75 ms: PoWeR- 75.4 ± 14.7 mN∗m/s, Control- 70.8 ± 18.1 mN∗m/s, $P = 0.5003$, ES = 0.28).

Similarities in gene expression between young and old soleus with PoWeR, but differences in the plantaris

We performed RNA-seq on soleus and plantaris muscles from old control and PoWeR mice, then compared these results to previously published RNA-seq from sex- and condition-matched young (4 mo old) PoWeR mice[31] (Supplemental Tables 2A–D). Tissue was collected after an overnight fast in all conditions and 24-h wheel lock in PoWeR mice. At the pathway level in the soleus, PoWeR was associated with over-representation of genes related to growth and remodeling (e.g., pathways in cancer, FoxO signaling, mTOR signaling) in both young and old mice relative to respective age-matched controls (Figure 7A and B). In young mice, genes in pathways related to ribosome synthesis

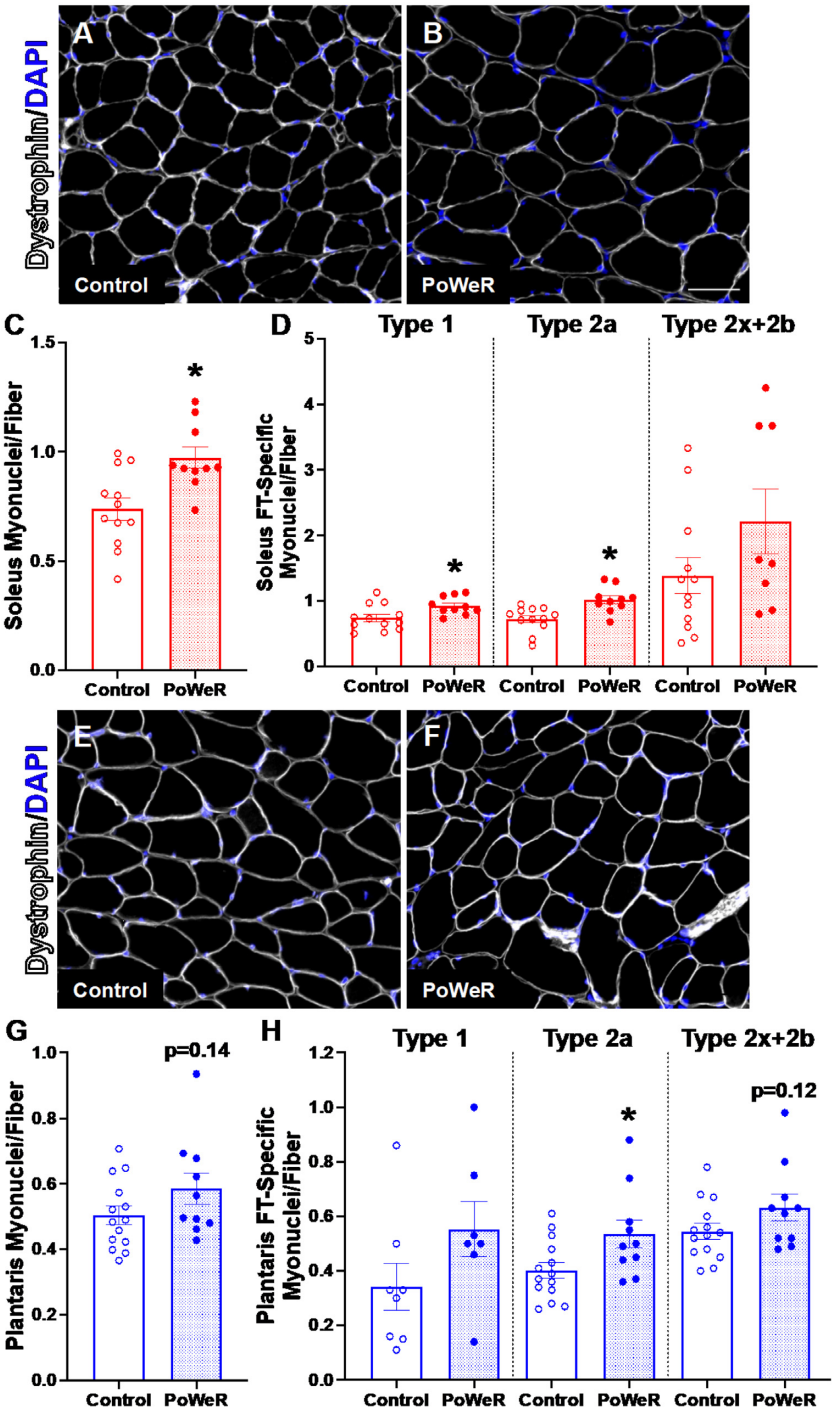

Figure 4. *Elevated fiber-type specific myonuclei following PoWeR.* Representative images of dystrophin (white) and DAPI (blue) IHC in the soleus from **(A)** control and **(B)** PoWeR trained old mice. **(C)** Quantification of soleus myonuclei per fiber. **(D)** Quantification of soleus fiber-type specific (Type 1, Type 2a, and Type 2x + 2b) myonuclei per fiber. Representative images of dystrophin (white) and DAPI (blue) IHC in the plantaris from **(E)** control and **(F)** PoWeR trained old mice. **(G)** Quantification of plantaris myonuclei per fiber. **(H)** Quantification of plantaris fiber-type specific (Type 1, Type 2a, and Type 2x + 2b) myonuclei per fiber. Open bars = control mice, dotted bars = PoWeR mice. $*$ indicates $P < 0.05$. Scale bars = 50 μm. Error bars represent SEM. N = 10–14 per group. Note: the same images from Figure 2 were used for myonuclear analysis in this Figure.

and oxidative metabolism were lower than controls (Figure 7C), consistent with our previous PoWeR studies in young mice.[31,34] Only oxidative metabolism-related genes were lower in old mice (Figure 7D). Generally, in response to PoWeR in the soleus, transcriptional responsiveness seemingly remained intact in muscle from aged mice. In the plantaris muscle, up-regulated genes in young PoWeR mice were primarily in FoxO, Erbb, IL-6, and EGFR1 pathways (Figure 7E), while in old PoWeR mice genes involved in gap junction and VEGF pathways were elevated (Figure 7F). Differential gene expression after training in the plantaris may underpin attenuated adaptations to PoWeR in young versus old mice.[24] Similar to the soleus, downregulated genes in the

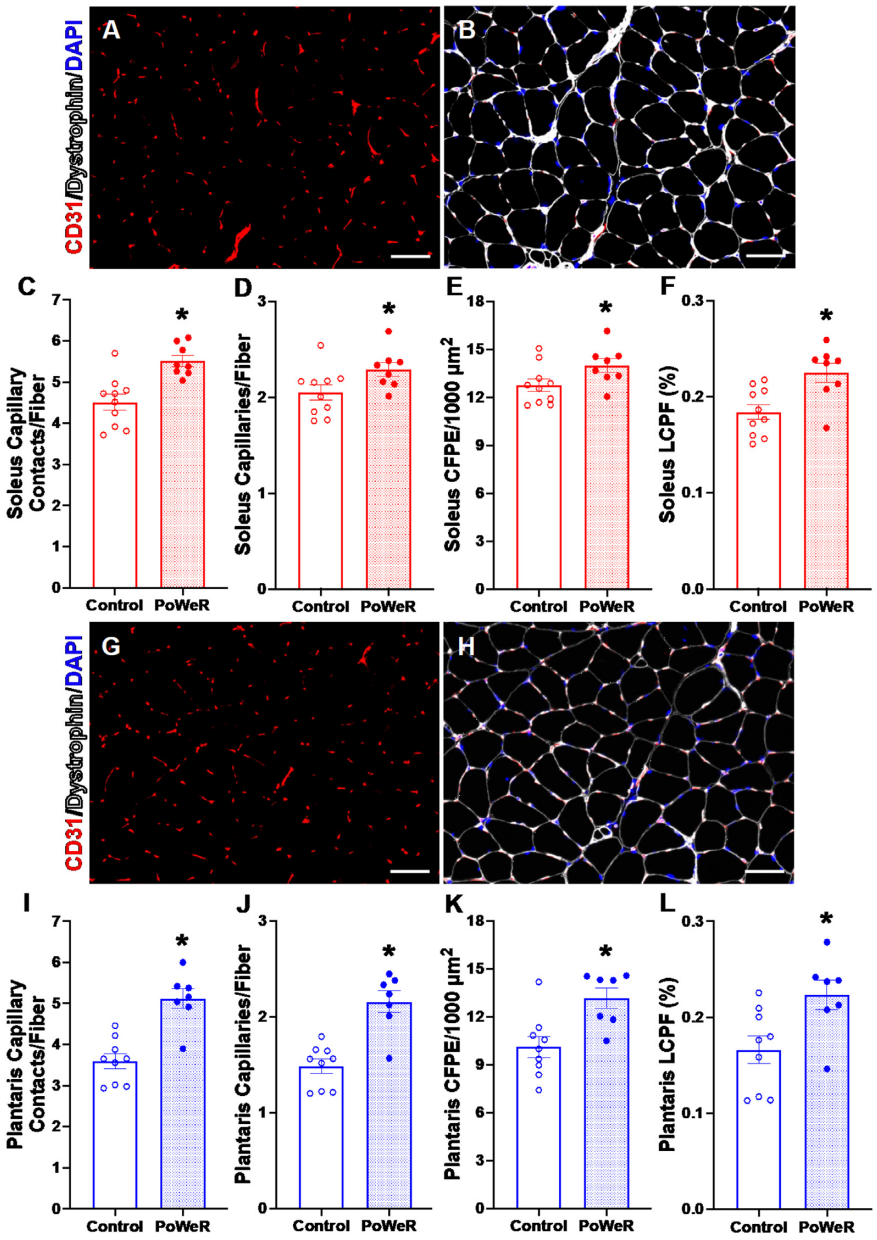

Figure 5. *Capillary content is augmented with PoWeR.* Representative images of **(A)** CD31 (red) and **(B)** CD31 (red), dystrophin (white), and DAPI (blue) IHC in the soleus from a PoWeR trained mouse. **(C)** Soleus capillary contacts per fiber. **(D)** Soleus capillary density normalized to fiber number. **(E)** Soleus CFPE per 1000 μm^2. **(F)** Percent soleus LCPF. Representative images of **(G)** CD31 (red) and **(H)** CD31 (red), dystrophin (white), and DAPI (blue) IHC in the plantaris from a PoWeR trained mouse. **(I)** Plantaris capillary contacts per fiber. **(J)** Plantaris capillary density normalized to fiber number. **(K)** Plantaris CFPE per 1000 μm^2. **(L)** Percent plantaris LCPF. CFPE = capillary to fiber perimeter exchange. LCPF = capillary to fiber interface. Open bars = control mice, dotted bars = PoWeR mice. $*$ indicates $P < 0.05$. Scale bars = 50 μm. Error bars represent SEM. N = 7–10 per group.

plantaris of young PoWeR mice were largely in ribosome-related pathways (Figure 7G). By contrast, very few genes and pathways were downregulated in the plantaris of old PoWeR mice (Figure 7H).

Conserved transcriptional features in soleus and plantaris muscles of young and aged mice with PoWeR

To gain insight into what may contribute to PoWeR adaptations in skeletal muscle at the molecular level, we searched for conserved genes across muscles and ages. Two genes, *Aldh1l1* and *Lrrn1*, were higher in both the soleus and plantaris in young and old mice in response to PoWeR (FDR < 0.05 Figure 7I). The abundance of these genes across muscles and conditions is reported in Figures 8A–D.

Myonuclear RRBS suggested coordinated regulation of dna methylation and gene expression after PoWeR

To provide information on what genes could be regulated at the epigenetic level with exercise in aged muscle, we conducted low-input RRBS on soleus myonuclei from untrained (n = 3) and PoWeR trained mice (n = 3) using our HSA-GFP model, as previously described.[33,34,50,52] HSA-GFP mice were treated the same as C57BL/6 mice above. PoWeR resulted in global myonuclear

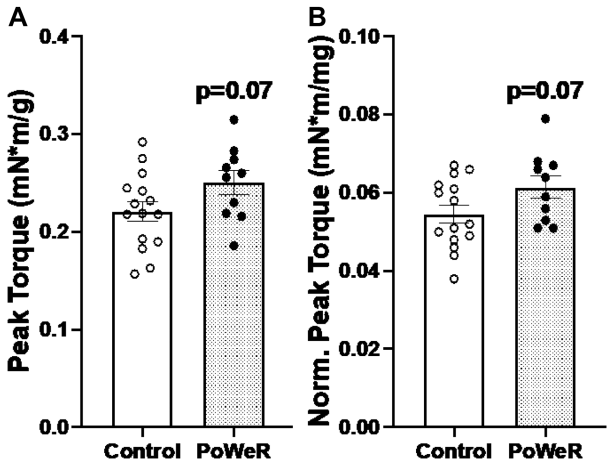

Figure 6. *Improvements in plantar flexion peak torque following PoWeR.* **(A)** Isometric peak tetanic torque of plantar flexors normalized to body weight. **(B)** Isometric peak tetanic torque of plantar flexors normalized to combined plantar flexor wet muscle weights. Open bars = control mice, dotted bars = PoWeR mice. Error bars represent SEM. N = 10–15 per group.

DNA CpG hypomethylation in promoters, exons, and introns (Figure 9A, Supplemental Tables 3A–C). The promoter region of *Rbm10* was hypomethylated by late-life PoWeR in the gastrocnemius [77], and a promoter CpG in myonuclear DNA of the soleus was similarly hypomethylated after PoWeR (29 ± 5% versus 9 ± 2%, FDR = 0.06, Supplemental Table 3). Since promoter CpG site methylation is generally inversely associated with gene expression,[57–61] we collated our aged soleus RNA-seq data with the myonuclear RRBS data. CpG hypomethylation in the promoter regions of 4 genes corresponded with higher transcript levels with PoWeR (*Agrn*, *Kat2a*, *Samd1*, and *Zfp598*, FDR < 0.10) (Figure 9B and C). CpG promoter region hypermethylation corresponded with lower transcript levels in four genes with PoWeR (*Ccnt*, *Gng5*, *Mylpf*, and *Slc25a20*, FDR < 0.10) (Figure 9D and E). The myonuclear methylation data point to specific epigenetic regulation of transcription during exercise within muscle fibers form aged mice.

Discussion

PoWeR is an easy-to-deploy and effective combined training modality for inducing pronounced skeletal muscle adaptations in aged mice. Compared to young C57BL/6 mice,[23,24,32] old mice run less (10–12 km/night versus 6-8 km/night) on a wheel that is only weighted to 5 g (as opposed to 6 g). Nevertheless, fiber type transitions, muscle fiber hypertrophy, satellite cell proliferation, and myonuclear accretion were still similar in magnitude between young and aged.[23,24,31,34]. Specifically, adaptations in the oxidative Type 2a fibers of the soleus, plantaris, and gastrocnemius were comparable (see Supplemental Table 1). Less hypertrophy in other fiber types may be attributable to the lower volume and/or loading in aged versus young PoWeR mice, or the potentially differential propensity of glycolytic fiber types to adapt with age. Attenuated growth specifically in the plantaris muscle could be attributable to its overall fiber type profile and/or the loading and recruitment pattern of this muscle. By contrast, in the soleus muscle that contains myosin fiber types more analogous to those found in humans (i.e., Type 1 and 2a) and where adaptations between young and old mice were comparable across fiber types despite differences in training (see Supplemental Table 1), the gene expression profile at the pathway level was similar (see Figure 7). These findings suggest continued muscle plasticity into old age with voluntary high-volume combined resistive training. Among the most striking observations was the angiogenic response to PoWeR in aged muscle. Recent work from our laboratory and others implicates angiogenesis as a potentially important but under-studied factor in muscle mass regulation during aging.[36,37,39–42] Angiogenesis as a hypertrophic moderator could be related to the secretory interplay with satellite cells and/or muscle fibers, the delivery of nutrients, or the removal of metabolic by-products from muscle.[38,39,62,63] The magnitude of angiogenesis with PoWeR exceeded what was recently reported with involuntary overload + forced run training in old mice.[19] Pre-clinical exercise models can be used to inform human interventions directed at preventing muscle mass and function loss with aging. The functional, cellular, and molecular data presented here can therefore be leveraged as a resource to help unravel the complex issue of sarcopenia and compromised plasticity with age in other muscle loading models.

Human concurrent training studies suggest that combined endurance and resistance training can elicit greater muscle hypertrophy than resistance training alone, at least in young untrained individuals.[21] Although PoWeR in mice is not directly comparable to concurrent training in humans where resistance and endurance exercise occurs in separate sessions, the effects of simultaneous adaptations are similar. One such similarity is the robust increase in myonuclear number observed with PoWeR across several muscles of different fiber type composition and function. Recent evidence suggests that accentuated hypertrophy with concurrent training relative to resistance training alone in humans is associated with higher myonuclear accretion from satellite cells.[64] In muscle from aged mice, loss-of-function studies suggest that myonuclear accretion does not drive short-term overload-induced hypertrophy,[16] but is at least permissive for hypertrophic muscle growth from exercise throughout the lifespan.[8] In the current investigation, muscle fiber hypertrophy was generally associated with satellite cell activity and myonuclear accretion, but not exclusively (e.g., Type 2x + 2b fibers of the plantaris). The uncoupling of load-induced hypertrophy from significant myonuclear accretion is not uncommon[65] and points to the multi-faceted role that satellite cells play during muscle adaptation.[66,67] Satellite cells reside in close proximity to capillaries.[68,69] Loss-of-function experiments indicate that satellite cell proliferation and/or myonuclear accretion is important for angiogenesis during load-induced hypertrophy.[70] Satellite cells may signal to endothelial cells via secretory signaling during mechanical overload in adult muscle.[63] Satellite cells also regulate intrafusal muscle fiber homeostasis and coordination during exercise.[8,71] Fusion-dependent as well as independent functions of satellite cells[63,72,73] related to endothelial cells and other cells of the niche (such as fibrogenic cells) may therefore support muscle adaptation in response to PoWeR in muscle of aged mice. Future analyses of concurrently trained muscle from aged mice and humans should broaden the scope of satellite cell contributions beyond myonuclear addition in order to understand and leverage the various pro-hypertrophic properties of muscle stem cells, [66] as well as the specific interplay with muscle vasculature.[62,68]

Aldh1l1 was recently identified as a source of oxidative stress in skeletal muscle fibers, the suppression of which facilitates adaptations to endurance training.[74] Interestingly, another recent study reported that *Aldh1l1* localizes conspicuously in vascular and angiogenic structures in skeletal muscle.[75] These findings motivated us to interrogate where *Aldh1l1* expression

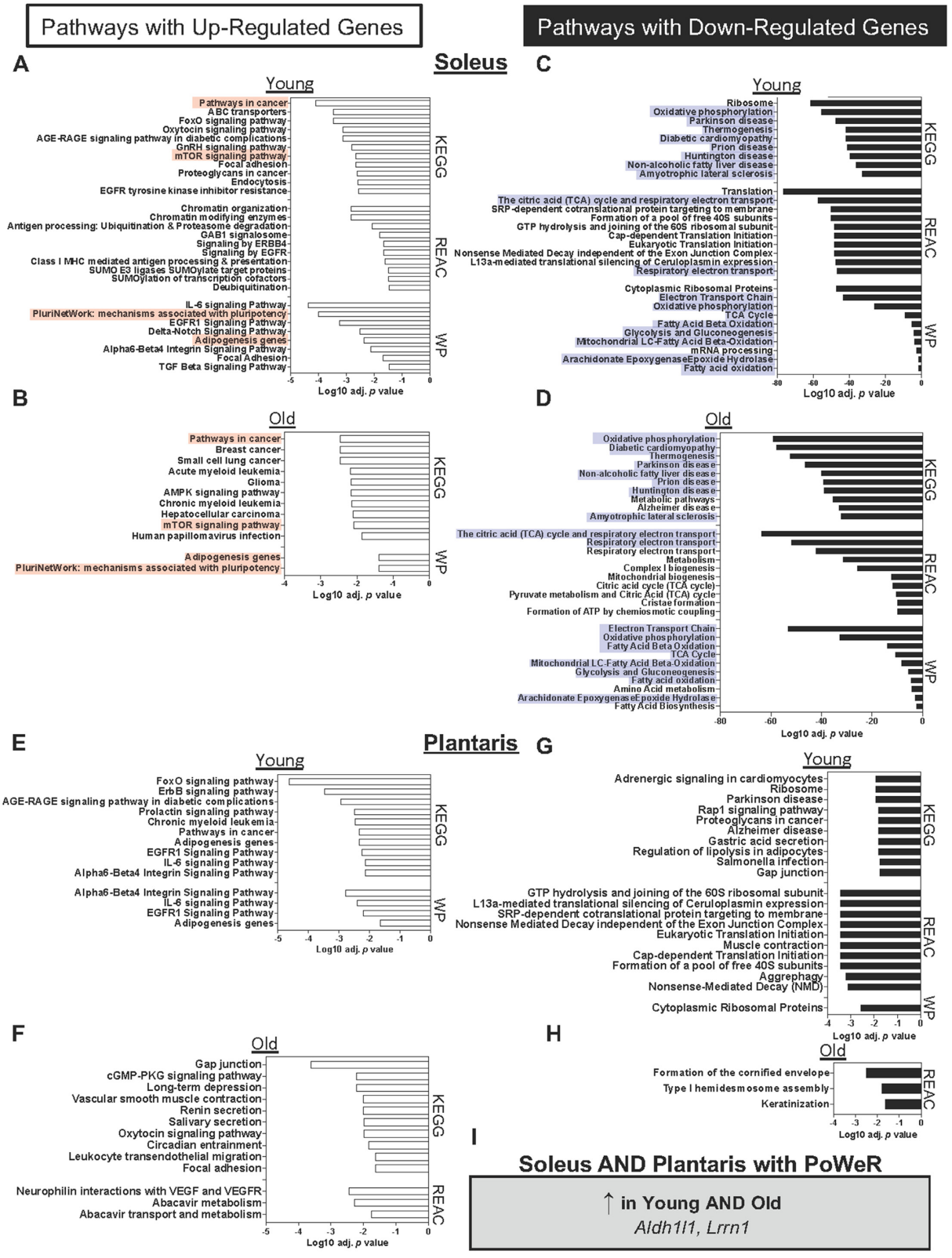

Figure 7. *Soleus and plantaris gene expression changes in young and old mice in response to PoWeR.* Over-representation analysis of pathways (adj. P<<0.05i>) with up-regulated genes after PoWeR in the soleus of **(A)** young and **(B)** old mice. Pathways with down-regulated genes after PoWeR in the soleus of **(C)** young and **(D)** old mice. Pathways with up-regulated genes after PoWeR in the plantaris of **(E)** young and **(F)** old mice. Pathways with down-regulated genes after PoWeR in the plantaris of **(G)** young and **(H)** old mice. **(I)** Genes that were up-regulated with PoWeR in all muscles and conditions. Open bars = young mice, solid bars = old mice. N = 4 young sedentary, 4 young PoWeR, 5 old sedentary, 4 old PoWeR per group. Red boxes indicate shared upregulated pathways between old and young; blue boxes indicate shared downregulated pathways.

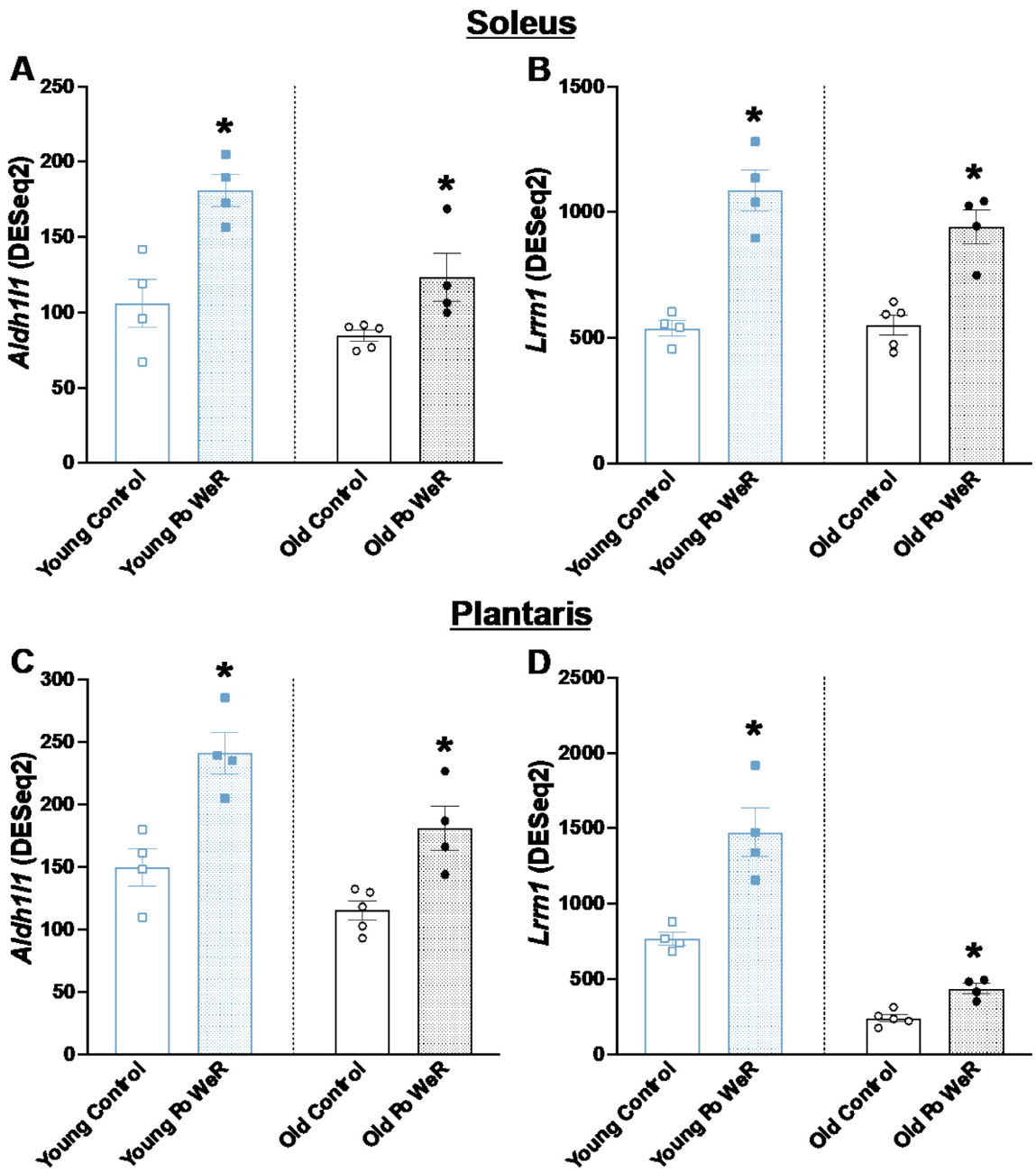

Figure 8. *Genes that were elevated in the soleus and plantaris of young and aged mice after PoWeR. Aldh1l1* transcript levels in the soleus of **(A)** young and **(B)** old mice. *Lrrn1* transcript levels in the plantaris of **(C)** young and **(D)** old mice. Open bars = control mice, dotted bars = PoWeR mice. ∗ indicates FDR < 0.10 versus respective age-matched control. Error bars represent SEM. N = 4–5 per group.

may occur in muscle during adaptation, since it was significantly elevated with PoWeR across muscles and ages in our study. We reanalyzed a single myonuclear sequencing dataset.[31,35] In addition to being expressed in myosin heavy chain Type IIB nuclei, found that *Aldh1l1* is primarily increased after PoWeR in endothelial cell nuclei of the soleus (Supplemental Figure 6A). As further evidence of a role for *Aldh1l1* in angiogenesis, we used a single-cell/nucleus RNA-seq database from the Cosgrove Laboratory (http://scmuscle.bme.cornell.edu/)[76] that contains information from 350 000 cells during regeneration. We confirmed that endothelial cells are the primary source of *Aldh1l1* expression in muscle (Supplemental Figure 6B). Four-day synergist ablation overload single cell RNA-sequencing data in young mice [63] similarly showed *Aldh1l1* to be expressed primarily in *Pecam1* + endothelial cells (Supplemental Figure 6C); all other populations had essentially no expression. Taken together, these data point to *Aldh1l1* playing some role in angiogenesis during muscle hypertrophy. The only other gene that was elevated with PoWeR across ages and muscles was *Lrrn1*. This gene is induced during developmental myogenesis,[77,78] but is also among the most elevated genes during *Sox6* knockout-mediated fiber type-switching to a predominantly slow-twitch phenotype.[79] Given the substantial faster-to-slower fiber type transition observed with PoWeR, we hypothesized that *Lrrn1* would be increased specifically in myonuclei in response to PoWeR. Indeed, single nucleus RNA-sequencing confirmed this

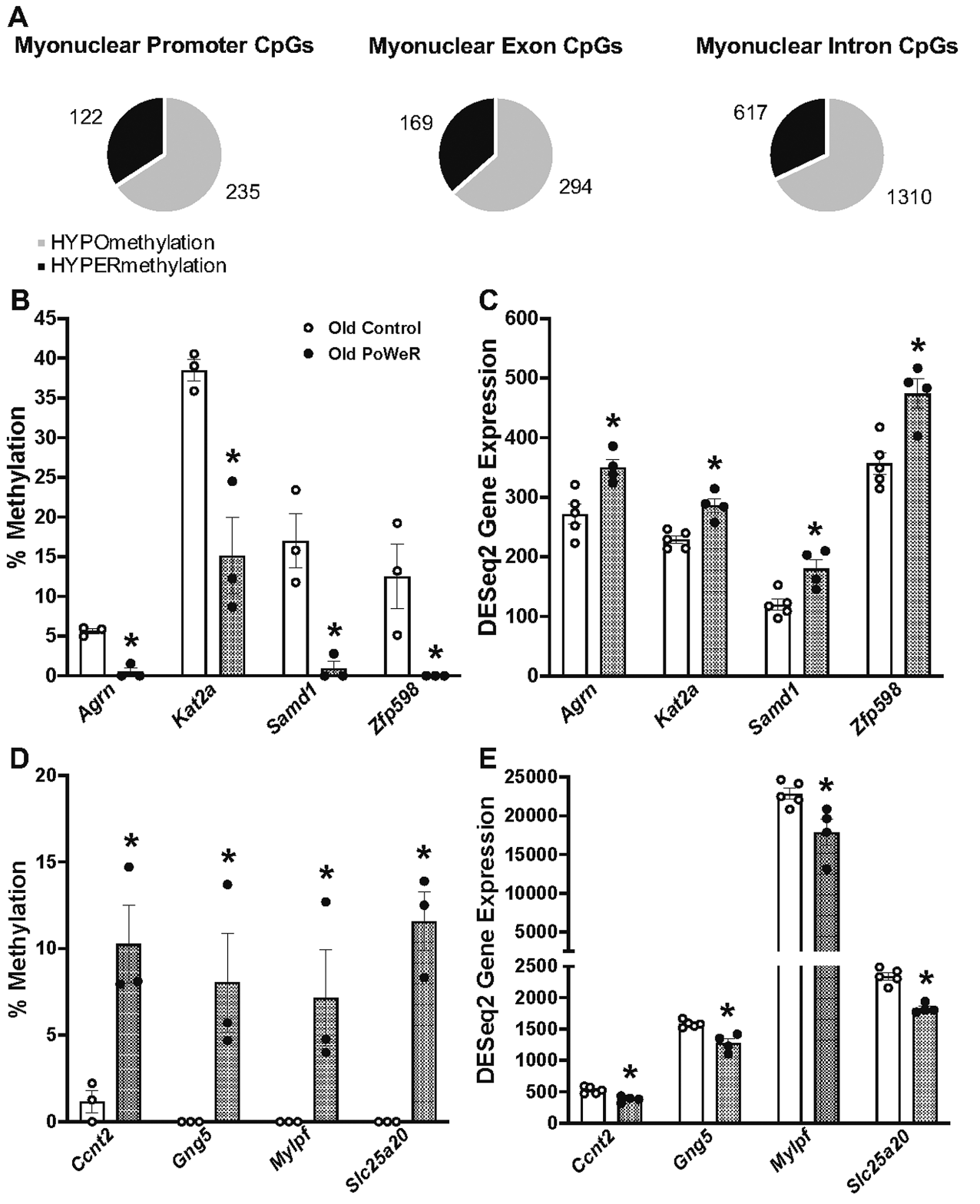

Figure 9. *Myonuclear DNA CpG methylation with PoWeR in aged mice and corresponding gene expression via RNA-seq.* **(A)** Distribution of myonuclear DNA methylation in promoter, exon, and intron regions of genes with PoWeR; multiple CpGs may be mapped to 1 gene (see Supplemental Table 2). **(B)** Genes with promoter CpG hypomethylation in soleus myonuclear DNA. **(C)** Corresponding genes with higher mRNA levels in soleus muscle of aged PoWeR mice. **(D)** Genes with promoter CpG hypermethylation in soleus myonuclear DNA. **(E)** Corresponding genes with lower mRNA levels in soleus muscle of aged PoWeR mice. Open bars = control mice, dotted bars = PoWeR mice. Green bars = HSA-GFP mice used for myonuclear RRBS. ∗ indicates FDR < 0.10 versus respective age-matched control. Error bars represent SEM. N = 3 HSA-GFP for myonuclear RRBS, 4–5 wild-type mice per group for RNA-seq.

to be the case in young PoWeR muscles (Supplemental Figure 6D).[35] *LRRN1* is modestly elevated in muscle tissue three hours after a heavy bout of endurance exercise in young well-trained men (logFC 0.85, FDR = 0.17, data from MetaMex)[80,81]. Since such exercise is known to elicit oxidative fiber type-transitioning, it would be informative to explore whether regulation occurs specifically in human myonuclei. The induction of *FN14* after acute exercise is associated with exercise-mediated fast-twitch hypertrophy in humans.[82,83] Gene expression of the TWEAK receptor *Fn14* (*Tnfrsf12a*) was appreciably lower after training in the soleus of young (FDR < 0.00001) and old mice (FDR < 0.00001), as well as young plantaris muscle with PoWeR (FDR = 0.07) (Supplemental Tables 2A–C). In the soleus, repression could be explained by the reduction of Type 2a fiber abundance in favor of Type 1 with PoWeR, but not in the plantaris. *Fn14* is expressed in myonuclei and responsive to acute exercise [35] but appears most enriched in satellite cells during damage-mediated muscle remodeling.[76] More work is needed to unravel how *Fn14* contributes to muscle adaptation.[84]

Late-life PoWeR mitigates skeletal muscle epigenetic aging in gastrocnemius muscle tissue and is specifically characterized by hypomethylation of promoter region CpGs.[85] By subjecting HSA-GFP mice to PoWeR from 22 to 24 mo of age, we could further interrogate myonuclear epigenetic regulation of gene expression with aging and exercise. In myonuclei, widespread hypomethylation across the genome was observed with PoWeR including in promoters, indicative of epigenetic plasticity with training in aged soleus muscle. We previously reported more youthful hypomethylated promoter region methylation levels of the splicing factor *Rbm10* [86] in gastrocnemius of aged mice after late-life PoWeR, which we confirmed with high-coverage targeted analysis.[85] Extending this finding, a CpG in the promoter region of *Rbm10* was hypomethylated by PoWeR in soleus myonuclei of aged mice. In young mice, *Rbm10* mRNA levels were 27% higher in the soleus after PoWeR (FDR = 0.10) but were not elevated after PoWeR in aged soleus (Supplemental Table 2). *Rbm10* promoter region methylation status could be a muscle fiber-specific biomarker of aging that is sensitive to rejuvenation by exercise. Of the genes where myonuclear methylation matched the anticipated direction of gene expression in aged mice, *Agrn* emerged as a target of interest in skeletal muscle that may be explicitly regulated with exercise. Agrin is a secreted factor with a well-characterized role in neuromuscular junction formation and stabilization,[87–90] can prevent atrophy in pathological conditions,[91] and potentially rescue denervation.[92] More recently, Agrin was implicated as a powerful stimulator of angiogenesis in tumors via crosstalk with endothelial cells.[93,94] We speculate that upregulation of *Agrn* in muscle fibers could contribute to neuromuscular junction remodeling as well as capillarization observed with PoWeR in aged mice. Given the localization and function of Agrin heavily relates to its splicing,[95,96] a deeper exploration of how Agrin mediates skeletal muscle adaptation to exercise at the protein level is warranted. *Samd1* also had a hypomethylated myonuclear promoter CpG concomitant with higher gene expression after PoWeR in aged mice. SAMD1 is a repressive chromatin regulator at unmethylated CpG islands,[97] but is also essential for angiogenesis.[98] Finally, a CpG in the promoter region of the genes encoding myosin heavy chain 2b (*Myh4*) and light chain 2b (*Mylpf*) were hypermethylated in myonuclei after PoWeR (FDR = 0.02 for both); the latter corresponds with lower gene expression. These data are consistent with evidence for the epigenetic control of myosin fiber type in adult muscle.[99,100] All of the myonuclear DNA CpGs assessed in this study are in Supplemental Table 3.

Our data collectively highlight how aged soleus muscle maintains plasticity with high-volume combined exercise training from the whole muscle to myonuclear epigenetic level. PoWeR is also associated with a significant increase in muscle capillarization that may help facilitate growth. Transcriptional analysis in bulk tissue with insights from single cells and nuclei points to *Aldh1l1* as a potentially important regulator of angiogenesis, while myonuclear-specific RRBS points to Agrin as a possible neuromuscular as well as angiogenic regulator in muscle with exercise. *Rbm10* promoter methylation could potentially serve as a readout of aging and exercise adaptation specifically in muscle fibers. Future investigations will determine whether further augmenting angiogenesis can facilitate greater hypertrophy with exercise during aging and the causal or permissive roles of *Aldh1l1* and *Agrn* in muscle adaptation. PoWeR can be leveraged as a simple and effective pre-clinical platform for discovering cellular and molecular regulators of muscle adaptation with aging, thereby driving the discovery of new therapeutics for aging-related muscle pathology.

Abbreviations list

PoWeR: progressive weighted wheel running; IHC: immunohistochemistry; PBS: phosphate buffered saline; NBT: nitrotetrazolium blue; SDH: succinate dehydrogenase; CS: citrate synthase; CCO: cytochrome c oxidase; RRBS: reduced representation bisulfite sequencing

Supplementary material

Supplementary material is available at the *APS Function* online.

Funding

Research reported in this publication was supported by the National Institute of Aging of the National Institutes of Health under Award Number R00 AG063994 to KAM. The content is solely the responsibility of the authors and does not represent the official views of the National Institutes of Health.

Acknowledgments

We wish to thank the staff of the Division of Laboratory Animal Resources at the University of Kentucky. We would like to thank Drs. Charlotte Peterson and John McCarthy for their intellectual and financial support for this project through NIH grants R01AG069909 and R01DK119619, the University of Kentucky Center for Muscle Biology for feedback on this work, and startup funds to Dr. Chris Fry from the College of Health Sciences. We would also like to thank Dr. Taylor Valentino for his technical assistance. The graphical abstract was generated using BioRender.

Author Contributions: CMD, CRB, and KAM conducted experiments and data analysis, generated figures, and drafted the manuscript. YW, CJZ, CL, NTT, AMZ, BDB, GLV, and ARK conducted experiments and data analysis. KAM and CSF oversaw successful completion of the study, assisted with data analysis, provided financial support, and prepared the manuscript and figures for submission. All authors read, edited, and approved of the final manuscript.

Conflict of Interest Statement

YW is sole proprietor of Myoanalytics LLC, and SJW is the Founder of Ridgeline Therapeutics. No other conflicts are declared.

Data Availability

RRBS data were deposited in Gene Expression Omnibus: GSE197045. RNA-sequencing data were deposited in Gene Expression Omnibus: GSE198652

References

1 Janssen I., Heymsfield S. B., Wang Z. M., Ross R. Skeletal muscle mass and distribution in 468 men and women aged 18- 81–88 yr. *J Appl Physiol* 2000; **89**,1, 81–88.

2 Janssen I., Shepard D. S., Katzmarzyk P. T., Roubenoff R. The healthcare costs of sarcopenia in the United States. *J Am Geriatr Soc* 2004;**52**,1, 80–85.

3 Moro T., et al. Muscle protein anabolic resistance to essential amino acids does not occur in healthy older adults before or after resistance exercise training. *J Nutr* 2018;**148**,6, 900–909.

4 Macaluso A., De Vito G. Muscle strength, power and adaptations to resistance training in older people. *Eur J Appl Physiol* 2004;**91**,4, 450–472.

5 Moro T., et al. Low skeletal muscle capillarization limits muscle adaptation to resistance exercise training in older adults. *Exp Gerontol* 2019;**127**, 110723.

6 Hunter G. R., McCarthy J. P., Bamman M. M. Effects of resistance training on older adults. *Sports Medicine* 2004;**34**,5, 329–348.

7 Harber M. P., et al. Aerobic exercise training improves whole muscle and single myofiber size and function in older women. *Am J Physiol-Regul, Integr Comp Physiol* 2009;**297**,5, R1452–R1459.

8 Englund D. A., et al. Depletion of resident muscle stem cells negatively impacts running volume, physical function and muscle hypertrophy in response to lifelong physical activity. *Am J Physiol-Cell Physiol* 2020;**318**,6, C1178–C1188.

9 Lavin K. M., et al. The importance of resistance exercise training to combat neuromuscular aging. *Physiology* 2019;**34**,2, 112–122.

10 Harper S. A., et al. Resveratrol and exercise combined to treat functional limitations in late life: a pilot randomized controlled trial. *Exp Gerontol* 2021;**143**, 111111.

11 Layne A. S., et al. Resveratrol and exercise to treat functional limitations in late life: design of a randomized controlled trial. *Contem Clin Trials Commun* 2017;**6**, 58–63.

12 Murach K. A., McCarthy J. J., Peterson C. A., Dungan C. M. Making mice mighty: recent advances in translational models of load-induced muscle hypertrophy. *J Appl Physiol* 2020;**129**,3, 516–521.

13 Kirby T. J., McCarthy J. J., Peterson C. A., Fry C. S. Synergist ablation as a rodent model to study satellite cell dynamics in adult skeletal muscle. *Skeletal Muscle Regeneration in the Mouse: Methods and Protocols* 2016;43–52.

14 Fry C. S., et al. Regulation of the muscle fiber microenvironment by activated satellite cells during hypertrophy. *FASEB J* 2014;**28**,4, 1654–1665.

15 McCarthy J. J., et al. Effective fiber hypertrophy in satellite cell-depleted skeletal muscle. *Development* 2011;**138**,17, 3657–3666.

16 Lee J. D., et al. Aged muscle demonstrates fiber-type adaptations in response to mechanical overload, in the absence of myofiber hypertrophy, independent of satellite cell abundance. *J Gerontol Ser A: Biolog Sci Med Sci* 2016;**71**,4, 461–467.

17 Stec M. J., et al. Randomized, four-arm, dose-response clinical trial to optimize resistance exercise training for older adults with age-related muscle atrophy. *Exp Gerontol* 2017;**99**, 98–109.

18 Hendrickse P. W., Krusnauskas R., Hodson-Tole E., Venckunas T., Degens H. Endurance exercise plus overload induces fatigue resistance and similar hypertrophy in mice irrespective of muscle mass. *Exp Physiol* 2020;**105**,12, 2110–2122.

19 Hendrickse P. W., Krusnauskas R., Hodson-Tole E., Venckunas T., Degens H. Regular endurance exercise of overloaded muscle of young and old male mice does not attenuate hypertrophy and improves fatigue resistance. *GeroScience* 2021;**43**,2, 741–757.

20 Liguori G. Medicine, A. C. o. S. *ACSM's guidelines for exercise testing and prescription*. 2021; Lippincott Williams & Wilkins. Philadelphia, PA.

21 Murach K. A., Bagley J. R. Skeletal muscle hypertrophy with concurrent exercise training: contrary evidence for an interference effect. *Sports Medicine* 2016;**46**,8, 1029–1039.

22 Schumann M., et al. Compatibility of concurrent aerobic and strength training for skeletal muscle size and function: an updated systematic review and meta-analysis. *Sport Med* 2021;1–12.

23 Dungan C. M., et al. Elevated myonuclear density during skeletal muscle hypertrophy in response to training is reversed during detraining. *Am J Physiol-Cell Physiol* 2019;**316**,5, C649–C654.

24 Murach K. A., et al. Muscle memory: myonuclear accretion, maintenance, morphology, and miRNA levels with training and detraining in adult mice. *J Cachexia, Sarcopenia Muscle* 2020;**11**,6, 1705–1722.

25 Soffe Z., Radley-Crabb H. G., McMahon C., Grounds M. D., Shavlakadze T. Effects of loaded voluntary wheel exercise on performance and muscle hypertrophy in young and old male C57Bl/6J mice. *Scand J Med Sci Sports* 2016;**26**,2, 172–188.

26 Call J. A., Mckeehen J. N., Novotny S. A., Lowe D. A. Progressive resistance voluntary wheel running in the mdx mouse. *Muscle Nerve* 2010;**42**,6, 871–880.

27 Graber T. G., Fandrey K. R., Thompson L. V. Novel individualized power training protocol preserves physical function in adult and older mice. *GeroScience* 2019;**41**,2, 165–183.

28 Seldeen K. L., et al. High intensity interval training improves physical performance and frailty in aged mice. *J Gerontol: Ser A* 2018;**73**,4, 429–437.

29 Zhu W. G., et al. Weight pulling: a novel mouse model of human progressive resistance exercise. *Cells* 2021;**10**,9, 2459.

30 Cui D., et al. A novel voluntary weightlifting model in mice promotes muscle adaptation and insulin sensitivity with simultaneous enhancement of autophagy and mTOR pathway. *FASEB J* 2020;**34**,6, 7330–7344.

31 Englund D., et al. Satellite cell depletion disrupts transcriptional coordination and muscle adaptation to exercise. *Function* 2020;**2**,1, zqaa033.

32 Valentino T. R., et al. Dysbiosis of the gut microbiome impairs mouse skeletal muscle adaptation to exercise. *J Physiol* 2021;**599**,21, 4845–4863.

33 Murach K. A., Dungan C. M., von Walden F., Wen Y. Epigenetic evidence for distinct contributions of resident and acquired myonuclei during long-term exercise adaptation

using timed in vivo myonuclear labeling. *Am J Physiol-Cell Physiol* 2022; **322**,1, C86–C93.
34 Wen Y., et al. Nucleus type-specific DNA methylomics reveals epigenetic "memory" of prior adaptation in skeletal muscle. *Function* **2**, 5,2021; zqab038.
35 Wen Y., et al. Myonuclear transcriptional dynamics in response to exercise following satellite cell depletion. *iScience* 2021;**24**,8, 102838.
36 Messa G., et al. Morphological alterations of mouse skeletal muscles during early ageing are muscle specific. *Exp Gerontol* 2019;**125**, 110684.
37 Barnouin Y., et al. Coupling between skeletal muscle fiber size and capillarization is maintained during healthy aging. *J Cachexia, Sarcopenia Muscle* 2017;**8**,4, 647–659.
38 Fujimaki S., et al. The endothelial Dll4–muscular Notch2 axis regulates skeletal muscle mass. *Nature Metabolism* 2022;**4**,2, 180–189.
39 Snijders T., et al. Muscle fibre capillarization is a critical factor in muscle fibre hypertrophy during resistance exercise training in older men. *J Cachexia, Sarcopenia Muscle* 2017;**8**,2, 267–276.
40 Moro T., et al. Low skeletal muscle capillarization limits muscle adaptation to resistance exercise training in older adults. *Exp Gerontol* **127**, 2019; 110723.
41 Verdijk L. B., Snijders T., Holloway T. M., LJ V. L. Resistance training increases skeletal muscle capillarization in healthy older men. *Med Sci Sports Exercise* 2016;**48**,11, 2157–2164.
42 Betz M., et al. Muscle fiber capillarization is associated with various indices of skeletal muscle mass in healthy, older men. *Exp Gerontol* 2021;**143**, 111161.
43 Ballak S. B., et al. Blunted angiogenesis and hypertrophy are associated with increased fatigue resistance and unchanged aerobic capacity in old overloaded mouse muscle. *Age* 2016;**38**,2, 39.
44 Larsen S., et al. Biomarkers of mitochondrial content in skeletal muscle of healthy young human subjects. *J Physiol* 2012;**590**,14, 3349–3360.
45 Meinild Lundby A. K., et al. Exercise training increases skeletal muscle mitochondrial volume density by enlargement of existing mitochondria and not de novo biogenesis. *Acta Physiologica* e12905, 2018;**222**,1, doi:10.1111/apha.12905.
46 Spinazzi M., Casarin A., Pertegato V., Salviati L., Angelini C. Assessment of mitochondrial respiratory chain enzymatic activities on tissues and cultured cells. *Nat Protoc* 2012;**7**,6, 1235–1246.
47 Latham C. M., Fenger C. K., White S. H. Differential skeletal muscle mitochondrial characteristics of weanling racing-bred horses. *J Anim Sci* 2019; **97**,8, 3193–3198.
48 Raudvere U., et al. g: profiler: a web server for functional enrichment analysis and conversions of gene lists (2019 update). *Nucleic Acids Res* 2019;**47**,W1, W191–W198.
49 Reimand J., et al. Pathway enrichment analysis and visualization of omics data using g: profiler, GSEA, Cytoscape and EnrichmentMap. *Nat Protoc* 2019;**14**,2, 482–517.
50 von Walden F., et al. The myonuclear DNA methylome in response to an acute hypertrophic stimulus. *Epigenetics* 2020;**15**,11, 1151–1162.
51 Iwata M., et al. A novel tetracycline-responsive transgenic mouse strain for skeletal muscle-specific gene expression. *Skeletal Muscle* 2018;**8**,1, 33.
52 Figueiredo V. C., et al. Genetic and epigenetic regulation of skeletal muscle ribosome biogenesis with exercise. *J Physiol* 2021;**599**,13, 3363–3384.
53 Park Y., Figueroa M. E., Rozek L. S., Sartor M. A. MethylSig: a whole genome DNA methylation analysis pipeline. *Bioinformatics* 2014;**30**,17, 2414–2422.
54 Wen Y., et al. MyoVision: software for automated high-content analysis of skeletal muscle immunohistochemistry. *J Appl Physiol* 2018;**124**,1, 40–51.
55 Viggars M. R., Wen Y., Peterson C. A., Jarvis J. C. Automated cross-sectional analysis of trained, severely atrophied and recovering rat skeletal muscles using MyoVision 2.0. *J Appl Physiol* 2022;**132**,3, 593–610.
56 Bloemberg D., Quadrilatero J. Rapid determination of myosin heavy chain expression in rat, mouse, and human skeletal muscle using multicolor immunofluorescence analysis. *PLoS One* 2012;**7**,4, e35273.
57 Siegfried Z., et al. DNA methylation represses transcription in vivo. *Nat Genet* 1999;**22**,2, 203–206.
58 Kang J. G., Park J. S., Ko J.-H., Kim Y.-S. Regulation of gene expression by altered promoter methylation using a CRISPR/Cas9-mediated epigenetic editing system. *Sci Rep* 2019;**9**,1, 1–12.
59 Busslinger M., Hurst J., Flavell R. DNA methylation and the regulation of globin gene expression. *Cell* 1983;**34**,1, 197–206.
60 Walsh C. P., Chaillet J. R., Bestor T. H. Transcription of IAP endogenous retroviruses is constrained by cytosine methylation. *Nat Genet* 1998;**20**,2, 116–117.
61 Cooper S. J., Trinklein N. D., Anton E. D., Nguyen L., Myers R. M. Comprehensive analysis of transcriptional promoter structure and function in 1% of the human genome. *Genome Res* 2006;**16**,1, 1–10.
62 Nederveen J. P., Betz M. W., Snijders T., Parise G. The importance of muscle capillarization for optimizing satellite cell plasticity. *Exerc Sport Sci Rev* 2021;**49**,4, 284–290.
63 Murach K. A., et al. Early satellite cell communication creates a permissive environment for long-term muscle growth. *iScience* 2021;**24**,4, 102372.
64 Lundberg T. R., et al. Early accentuated muscle hypertrophy is strongly associated with myonuclear accretion. *J Appl Physiol* 2020; **319**, R50–R58.
65 Murach K. A., Englund D. A., Dupont-Versteegden E. E., McCarthy J. J., Peterson C. A. Myonuclear domain flexibility challenges rigid assumptions on satellite cell contribution to skeletal muscle fiber hypertrophy. *Front Physiol* 2018;**9**, 635, doi:10.3389/fphys.2018.00635.
66 Murach K. A., Fry C. S., Dupont-Versteegden E. E., McCarthy J. J., Peterson C. A. Fusion and beyond: satellite cell contributions to loading-induced skeletal muscle adaptation. *FASEB J* 2021;**35**,10, e21893.
67 Murach K. A., et al. Starring or supporting role? Satellite cells and skeletal muscle fiber size regulation. *Physiology* 2018;**33**,1, 26–38.
68 Nederveen J. P., et al. Skeletal muscle satellite cells are located at a closer proximity to capillaries in healthy young compared with older men. *J Cachexia, Sarcopenia Muscle* 2016;**7**,5, 547–554.
69 Christov C., et al. Muscle satellite cells and endothelial cells: close neighbors and privileged partners. *Mol Biol Cell*;2007, **18**,4, 1397–1409.
70 Ato S., Fukada S.-I., Kokubo H., Ogasawara R. Implication of satellite cell behaviors in capillary growth via VEGF expression-independent mechanism in response to mechanical loading in HeyL-null mice. *Am J Physiol-Cell Physiol* 2022; **322**,2, C275–C282.

71 Jackson J. R., et al. Reduced voluntary running performance is associated with impaired coordination as a result of muscle satellite cell depletion in adult mice. *Skeletal Muscle* 2015;**5**,1, 41, doi:10.1186/s13395-015-0065-3.

72 Murach K. A., et al. Fusion-independent satellite cell communication to muscle fibers during load-induced hypertrophy. *Function* 2020;**1**,1, zqaa009.

73 Fry C. S., Kirby T. J., Kosmac K., McCarthy J. J., Peterson C. A. Myogenic progenitor cells control extracellular matrix production by fibroblasts during skeletal muscle hypertrophy. *Cell Stem Cell* 2017;**20**,1, 56–69.

74 Villivalam S. D., et al. A necessary role of DNMT3A in endurance exercise by suppressing ALDH1L1-mediated oxidative stress. *EMBO J* 2021; e106491.

75 Etienne J., et al. Aldehyde dehydrogenases contribute to skeletal muscle homeostasis in healthy, aging, and Duchenne muscular dystrophy patients. *J Cachexia, Sarcopenia Muscle* 2020;**11**,4, 1047–1069.

76 McKellar D. W., et al. Large-scale integration of single-cell transcriptomic data captures transitional progenitor states in mouse skeletal muscle regeneration. *Commun Biol* 2021;**4**,1, 1–12.

77 Kaspar P., et al. c-Myb inhibits myoblast fusion. *PLoS One* 2013;**8**,10, e76742.

78 Seale P., Ishibashi J., Holterman C., Rudnicki M. A. Muscle satellite cell-specific genes identified by genetic profiling of MyoD-deficient myogenic cells. *Dev Biol* 2004;**275**,2, 287–300.

79 Quiat D., et al. Concerted regulation of myofiber-specific gene expression and muscle performance by the transcriptional repressor Sox6. *Proc Natl Acad Sci* 2011;**108**,25, 10196–10201.

80 Neubauer O., et al. Transcriptome analysis of neutrophils after endurance exercise reveals novel signaling mechanisms in the immune response to physiological stress. *J Appl Physiol* 2013;**114**,12, 1677–1688.

81 Pillon N. J., et al. Transcriptomic profiling of skeletal muscle adaptations to exercise and inactivity. *Nat Commun* 2020;**11**,1, 1–15.

82 Murach K., et al. Single muscle fiber gene expression with run taper. *PLoS One* 2014; **9**,9, e108547.

83 Raue U., et al. Transcriptome signature of resistance exercise adaptations: mixed muscle and fiber type specific profiles in young and old adults. *J Appl Physiol* 2012;**112**,10, 1625–1636.

84 Pascoe A. L., Johnston A. J., Murphy R. M. Controversies in TWEAK-Fn14 signaling in skeletal muscle atrophy and regeneration. *Cell Mol Life Sci* 2020; 1–13.

85 Murach K. A., et al. Late-life exercise mitigates skeletal muscle epigenetic aging. *Aging Cell* 2021; 13527.

86 Inoue A. RBM10: structure, functions, and associated diseases. *Gene* 2021, **783**, 145463.

87 McMahan U. J., et al. Agrin isoforms and their role in synaptogenesis. *Curr Opin Cell Biol* 1992;**4**,5, 869–874.

88 Hoch W. Formation of the neuromuscular junction: agrin and its unusual receptors. *Eur J Histochem* 1999;**265**, 1–10.

89 Florian Bentzinger C., Barzaghi P., Lin S., Ruegg M. A. Overexpression of mini-agrin in skeletal muscle increases muscle integrity and regenerative capacity in laminin-α2-deficient mice. *FASEB J* 2005;**19**,8, 934–942.

90 Bezakova G., Ruegg M. A. New insights into the roles of agrin. *Nat Rev Mol Cell Biol* 2003;**4**,4, 295–309.

91 Boido M., et al. Increasing agrin function antagonizes muscle atrophy and motor impairment in spinal muscular atrophy. *Front Cell Neurosci* 2018;**12**, 17.

92 Lin S., et al. Muscle-wide secretion of a miniaturized form of neural agrin rescues focal neuromuscular innervation in agrin mutant mice. *Proc Natl Acad Sci* 2008;**105**,32, 11406–11411.

93 Chakraborty S., Njah K., Hong W. Agrin mediates angiogenesis in the tumor microenvironment. *Trends Cancer* 2020;**6**,2, 81–85.

94 Njah K., et al. A role of agrin in maintaining the stability of vascular endothelial growth factor receptor-2 during tumor angiogenesis. *Cell Rep* 2019;**28**,4, 949–965.e7. e947.

95 Ferns M. J., Campanelli J. T., Hoch W., Scheller R. H., Hall Z. The ability of agrin to cluster AChRs depends on alternative splicing and on cell surface proteoglycans. *Neuron* 1993;**11**,3, 491–502.

96 Burgess R. W., Nguyen Q. T., Son Y.-J., Lichtman J. W., Sanes J. R. Alternatively spliced isoforms of nerve-and muscle-derived agrin: their roles at the neuromuscular junction. *Neuron* 1999;**23**,1, 33–44.

97 Stielow B., et al. The SAM domain-containing protein 1 (SAMD1) acts as a repressive chromatin regulator at unmethylated CpG islands. *Sci Adv* 2021;**7**,20, eabf2229.

98 Campbell B., Engle S., Bourassa P., Aiello R. Ablation of SAMD1 in mice causes failure of angiogenesis, embryonic lethality. *bioRxiv* 2022.

99 Begue G., Raue U., Jemiolo B., Trappe S. DNA methylation assessment from human slow-and fast-twitch skeletal muscle fibers. *J Appl Physiol* 2017;**122**,4, 952–967.

100 Oe M., Ojima K., Muroya S. Difference in potential DNA methylation impact on gene expression between fast-and slow-type myofibers. *Physiol Genomics* 2021;**53**,2, 69–83.